LETTER

Atmospheric Exposure Triggers Light-Induced Degradation in 2D Lead-Halide Perovskites

Gianluca Grimaldi, Imme Schuringa, Jaco J. Geuchies, Susan A. Rigter, Tom Hoekstra, Jan Versluis, Juanita Hidalgo, Juan-Pablo Correa-Baena, Jorik van de Groep, Heejae Kim, Mischa Bonn, and Bruno Ehrler*

Read Online

ACCESS | Metrics & More | Article Recommendations | Supporting Information

ABSTRACT: Quasi-2D perovskites have been pivotal in recent efforts to stabilize perovskite solar cells. Despite the stability boost provided when these materials are introduced in perovskite solar cells, little is known about the intrinsic light and environmental stability of quasi-2D perovskites. In this study, we characterize the photostability of exfoliated quasi-2D perovskite single crystals in air using photoluminescence, infrared, X-ray fluorescence, and energy-dispersive X-ray spectroscopy. Photoexcitation leads to severe material loss with oxygen as a prerequisite for material breakdown. The effect can be traced to the formation of reactive oxygen species, as demonstrated by increases in the photostability under oxygen-free conditions. We show the effect of combined passivation steps, showcasing the stability enhancement offered by 2D-capping layers in combination with an oxygen-free atmosphere. Our results reveal that the stability of illuminated quasi-2D perovskites depends critically on oxygen exposure, highlighting the importance of oxygen-blocking passivation strategies for stable 2D perovskite-based devices.

Quasi-2D perovskites

20 μm

Light + oxygen
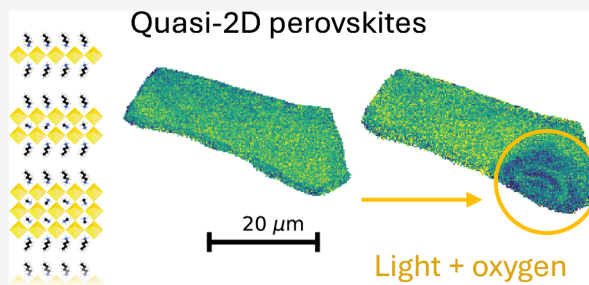
The rapid advance in perovskite photovoltaics has pushed this technology from impractical proof-of-concept devices to the brink of commercialization in the span of a decade.[1] Perovskite solar cells can now be fabricated with efficiencies comparable to those of single-crystalline silicon solar cells, shifting the technological bottleneck away from performance and toward stability. In the search for more stable perovskite compositions, low-dimensional perovskites have been identified as an attractive material candidate, and solar cell stacks featuring low-dimensional perovskites alongside conventional (3D) perovskites have demonstrated a remarkable combination of performance and stability. In particular, the 2D Ruddlesden–Popper phases, commonly known as two-dimensional (2D) perovskites, have been the focus of extensive research in the last couple of years, as incorporating a layer of 2D perovskites between a 3D perovskite light-absorber and a transport layer can lead to >20% efficiency solar cells with an operational lifetime of over 1000 h.[2−8]

The rationale behind the stabilization effect can be found in the structural properties of 2D perovskites, characterized by 2D layers of lead halide octahedra separated by layers of long organic molecules, called spacers. These materials can be classified by the number n of octahedral monolayers sandwiched between two spacer layers, where $n = 1$ is often

referred to as a 2D perovskite proper and $1 < n < 10$ is often called quasi-2D perovskite[9] (see Figure 1a). Perovskites with different n-values display substantial variations in electronic and optical properties,[10,11] due to quantum- and dielectric-confinement of the electronic wave functions in the 2D layers. These materials show increased hydrophobicity compared to their 3D counterparts, which is hypothesized to enhance their resistance to moisture-induced degradation processes prevalent in 3D perovskites.[2,12,13] Additionally, evidence of reduced ionic mobility in (quasi-) 2D perovskites in the dark[14,15] and under illumination[16,17] suggest incorporating these materials in a perovskite solar cell might mitigate degradation processes triggered by ion migration, such as ionic reactions with contacts and transport layers.

These properties are prompting researchers in the perovskite solar cell community to consider (quasi-) 2D perovskites as stable alternatives to 3D perovskites. However, recent reports
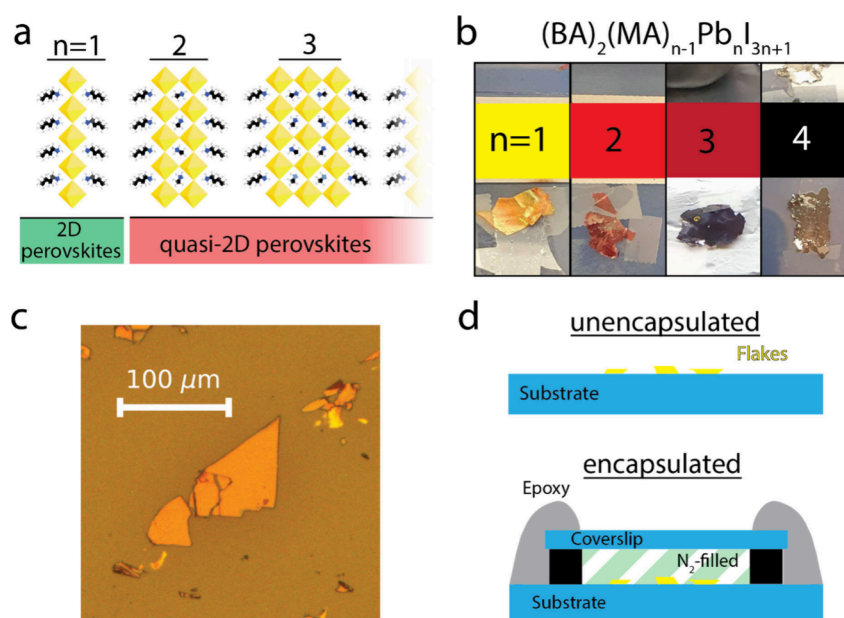
Figure 1. Preparation of (quasi-) 2D perovskite samples. (a) Schematics depicting the crystal structure of $(BA)_2(MA)_{n-1}Pb_nI_{3n+1}$. (b) Pictures of the (quasi-) 2D perovskite crystals used in this work. (c) Optical microscope image of exfoliated $n = 2$ flakes. (d) Schematics representing the sample geometry with and without the encapsulation step.

have cast doubts on the degree of stability of (quasi-) 2D perovskites exposed to heat,[18] intense illumination,[19,20] and vacuum,[21] conditions relevant for solar cell operation or fabrication. In particular, Fang et al. have highlighted the rapid photodegradation process affecting single crystals of $(PEA)_2PbI_4$, an $n = 1$ 2D perovskite. Upon illumination, the crystals undergo morphological and photoluminescence changes, attributed to the degradation of the 2D perovskite and the formation of PbI_2.[19]

Despite these warning signs, little is known about the intrinsic photostability of $n > 1$ quasi-2D perovskites, the versions of the material predominantly present in solar cell architectures. Furthermore, while applying passivation layers on top of $n = 1$ 2D perovskite crystals has been shown to increase their photostability,[19,22] the effect has been attributed to a reduction in photoinduced desorption of volatile species from the crystals,[19] without clarifying the role of airborne species (i.e., O_2, H_2O). Disentangling the impact of quasi-2D perovskite photostability from the complex system of electronic and ionic processes affecting 2D/3D solar cells is necessary to understand stability trends in these devices and to guide the design of stable perovskite solar cell architectures.

In this study, we investigate the stability of single crystals of $(BA)_2(MA)_{n-1}Pb_nI_{3n+1}$ (quasi-) 2D perovskites ($n = 1, ..., 4$) under laser illumination. We monitor local morphological and optical changes using a combination of photoluminescence (PL) microscopy, time-resolved PL imaging, optical microscopy, scanning electron microscopy-based energy dispersive X-ray (SEM/EDX) spectroscopy, Fourier-transform infrared (FTIR) spectroscopy, and X-ray fluorescence (XRF) imaging. Our results show that quasi-2D perovskites suffer from rapid photodegradation processes comparable to those affecting the $n = 1$ 2D perovskite species, leading to PL decay and material loss in the photoexcited spots. To elucidate the degradation mechanism, we monitored the evolution of the crystals exposed to different atmospheres, revealing the crucial role of oxygen in facilitating morphological and photoluminescence

changes. Illuminating in the absence of O_2 prevents morphology changes entirely in $n > 1$ quasi-2D perovskites, leading to milder PL losses attributed to the formation of electronic traps. Finally, we show that a combination of an O_2-free atmosphere and applying a 2D capping layer increases the photostability, suggesting the presence of both intrinsic (volatile species desorption) and extrinsic (O_2-induced) degradation pathways.

In order to obtain flakes of (quasi-) 2D perovskite materials, we synthesized centimeter-sized crystals of $(BA)_2(MA)_{n-1}Pb_nI_{3n+1}$ (BA = butylammonium, MA = methylammonium), with $n = 1, ..., 4$ (see Figure 1b). The material is pure-phase (only the nominal n-value present) for $n = 1$, and photoluminescence spectra from $n = 2-4$ are dominated by the nominal n-value (see Figure S1, Supporting Information). The large crystals were mechanically exfoliated in a nitrogen-filled glovebox using a tape-based exfoliation method commonly used for van der Waals 2D materials and then stamped on a glass substrate. The procedure resulted in the transfer of thin (a few hundred nanometers thick) flakes on the substrate, with lateral dimensions extending for tens of micrometers (see Figure 1c). The large lateral extension of the flakes allows the photoexcitation of selected spots on a single flake with a PL microscope, enabling direct comparison of the morphological and compositional characteristics of photoexcited spots with those of adjacent unexcited areas.

To determine the impact of air on the photostability of (quasi-) 2D perovskites, we prepare two sets of samples: one prepared via the exfoliating/stamping procedure described above and the second featuring an additional encapsulation step performed in the glovebox. The encapsulation allows optical measurements outside of the glovebox while maintaining the flakes in an O_2- and H_2O-free atmosphere. To encapsulate the samples, we place a 170 μm thick glass coverslip on top of the area with the stamped crystals, and we separate it from the substrate by strips of carbon tape. The edges of the coverslip are then covered with UV-cured epoxy,
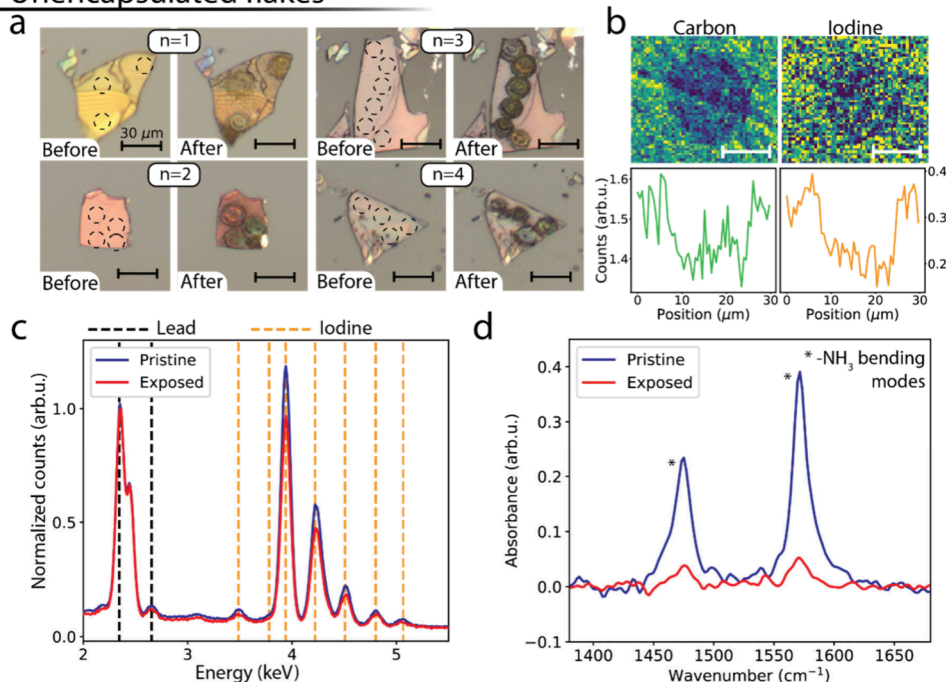
Figure 2. Morphology and compositional changes in unencapsulated flakes. (a) Optical microscope images of n = 1, ..., 4 flakes before and after local photoexcitation, showing the presence of color changes in the photoexcited spots. (b) EDX maps of a photoexcited spot in an n = 2 flake, displaying the spatial variations in the carbon (top-left) and iodine signals (top-right). The scale bars are 10 μm wide. The bottom panels show a horizontal crosscut of the signal shown in the top panels. (c) Spectrally resolved EDX signal, spatially integrated over the exposed area shown in (b) and over a pristine area of the same flake. (d) FTIR signal measured on an exposed and a pristine area of an n = 1 flake, shown in the spectral range containing peaks associated with BA vibrational modes.

sealing it to the substrate (see Figure 1d). The resulting airtight enclosure is filled with nitrogen to assess degradation without air and water, or with dry air to isolate the effect of O_2. This last sample also helps to distinguish between protection by the glass capping layer and removal of the O_2.

To characterize the stability of the unencapsulated flakes, we exposed flakes with different n-values to 405 nm laser light in a photoluminescence (PL) microscopy setup, allowing local photoexcitation of 15 μm wide spots on the flakes, while measuring the evolution of the PL during the exposure period. We exposed multiple spots on each flake using a fixed exposure time (~180 s) and varying laser fluence (spanning the range from 2.2×10^{18} to 4.5×10^{19} photons/(s cm^2)), to investigate the dependence of photodegradation effects on the incident energy dose. Figure 2a shows optical microscopy images of n = 1 to n = 4 flakes, comparing their morphology before and after localized photoexcitation (photoexcited spots highlighted with dashed circles). All flakes show signs of local morphology changes in the photoexcited spots, revealed by the appearance of a clear contrast compared to the unexposed part of the flakes. We note a color change of the flakes next to the excited spots on the n = 1 and n = 2 flakes, which we tentatively attribute to surface reactions with volatile species emitted from the photoexcited areas, as the effect seems to extend to neighboring flakes (Figure S2). Nevertheless, the excitation spots show the most prominent color changes for all of the n-values, suggesting local compositional changes. Since the effect is observed even at the lowest fluence measured, with a photon flux 4 times the average AM1.5 value,[23] it has the potential to affect quasi-2D perovskite solar cells in high-irradiance conditions.

To investigate changes in the composition of the flakes following photoexcitation, we performed scanning electron microscopy/energy dispersive X-ray (SEM/EDX) measurements on photoexcited unencapsulated flakes. Figure 2b shows an EDX map of an n = 2 flake, with the EDX signal integrated over a carbon peak (top-left panel) and an iodine peak (top-right panel), while the bottom panels show horizontal cross-cuts of the signal for each map. Both images show a decrease in signal intensity in correspondence with the photoexcited spot, suggesting that the morphology changes observed in optical images occur with a significant loss of iodine and organic components. An increase in the lead signal in the photoexcited area is also observed (Figure S3), consistent with a higher lead density in the decomposition product. Figure 2c shows an overview of the lead and iodine peaks in the EDX spectrum integrated over the exposed and pristine areas of the flake, normalized by the intensity of the highest lead peak to reveal variations in the I/Pb ratio. X-ray fluorescence (XRF) measurements on a photoexcited n = 3 flake show a similar reduction of the iodine component (Figure S4). The decrease in the I-peak intensities in the photoexcited area reveals a relative loss of iodine compared to the lead component, indicating the formation of volatile iodine species upon photoexcitation. Similar volatile iodine species have been reported in analogous systems.[19,21] We performed FTIR measurements to monitor changes in the organic components found in the photoexcited spots. Figure 2d shows FTIR measurements obtained on the exposed and pristine region of an n = 1 flake, focusing on the presence of sharp peaks in a spectral region compatible with vibrational modes of the BA spacer cation (Figures S5–S7). The intensity of the peaks is
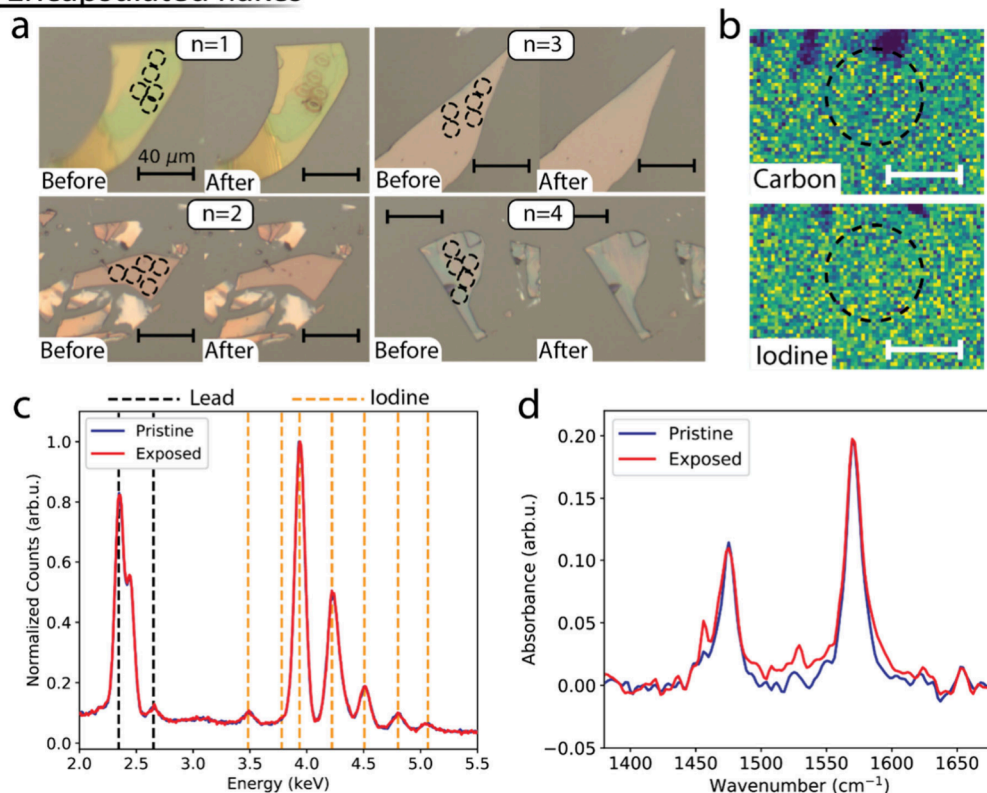
Encapsulated flakes

Figure 3. Morphology and compositional changes in encapsulated flakes. (a) Optical microscope images of $n = 1, ..., 4$ flakes before and after local photoexcitation, showing reduced morphology changes in the $n = 1$ flake and no change in the $n > 1$ flakes. (b) EDX maps of a photoexcited spot in an $n = 2$ flake, showing a lack of spatial variations in the carbon (top) and iodine signals (bottom) between exposed and pristine areas. The scale bars are 7 μm wide. (c) Spectrally resolved EDX signal, spatially integrated over the exposed area shown in (b) and over a pristine area of the same flake. (d) FTIR signal measured on an exposed and a pristine area of an $n = 1$ flake photoexcited in a N_2 atmosphere.

strongly suppressed after photoexcitation, indicating a high degree of organic component loss in the photoexcited areas. Despite the low sensitivity of EDX measurements to low atomic number components like carbon, a similar decrease is observed for the C/Pb ratio in the EDX measurements (Figure S3b).

These morphological and compositional observations on $n = 1$ and $n > 1$ flakes are compatible with a degradation mechanism proposed for phenethylammonium-based $n = 1$ 2D perovskites,[19,21] involving the conversion of illuminated 2D perovskite flakes into PbI_2, accompanied by the formation of volatile iodine and carbon byproducts. In the proposed reaction, the illuminated 2D perovskite decomposes without the involvement of external species, and the stability improvement observed when stacking a protecting material on top of the flakes was attributed to decreased desorption of the volatile reaction products.[19] However, the impact of O_2 and H_2O on the dynamics and nature of the degradation has not yet been assessed, despite the crucial role these species play in the photostability of 3D perovskites.[24−27]

To ascertain the role played by ambient exposure in the degradation process, we repeated for the encapsulated samples the same measurements discussed above. These measurements allow for the photoexcitation of the flakes in a nitrogen atmosphere without restricting the evaporation of volatile degradation products. Figure 3a shows optical images of (quasi-) 2D perovskite flakes taken before and after local

photoexcitation (laser fluences in the same range used in Figure 2). Looking at the comparison, it is evident that encapsulation drastically reduces the photoinduced morphological changes. While subtle contrast changes in the photoexcited spots remain apparent for the $n = 1$ flake, $n > 1$ quasi-2D perovskite flakes do not show morphology changes, nor is there evidence of the long-range changes that we observe in the unencapsulated $n = 1$ and $n = 2$ samples. No evidence of compositional change is observed in spatially (Figure 3b) and spectrally resolved (Figure 3c) EDX measurements on exposed and pristine areas of an $n = 2$ flake. Figure 3d shows the FTIR peaks associated with BA vibrational modes in an $n = 1$ flake, revealing a negligible signal change between a pristine area and an area photoexcited under N_2 atmosphere. A similar lack of changes in the FTIR peaks associated with BA vibrational modes is observed in quasi-2D $n = 2$ flakes photoexcited under an N_2 atmosphere (Figure S6). Our results demonstrate that the presence of air plays an active role in the photodegradation process. Additionally, a nitrogen atmosphere leads to complete prevention of material losses in $n > 1$ flakes upon photoexcitation.

While atmospheric control leads to strong suppression of the morphological and compositional changes, its impact on the optical property changes after photoexcitation appears more nuanced. Figures 4a−d shows the PL intensity obtained during laser exposure of $n = 1$ to $n = 4$ flakes, plotted as a function of the radiation energy dose received during exposure (i.e.,
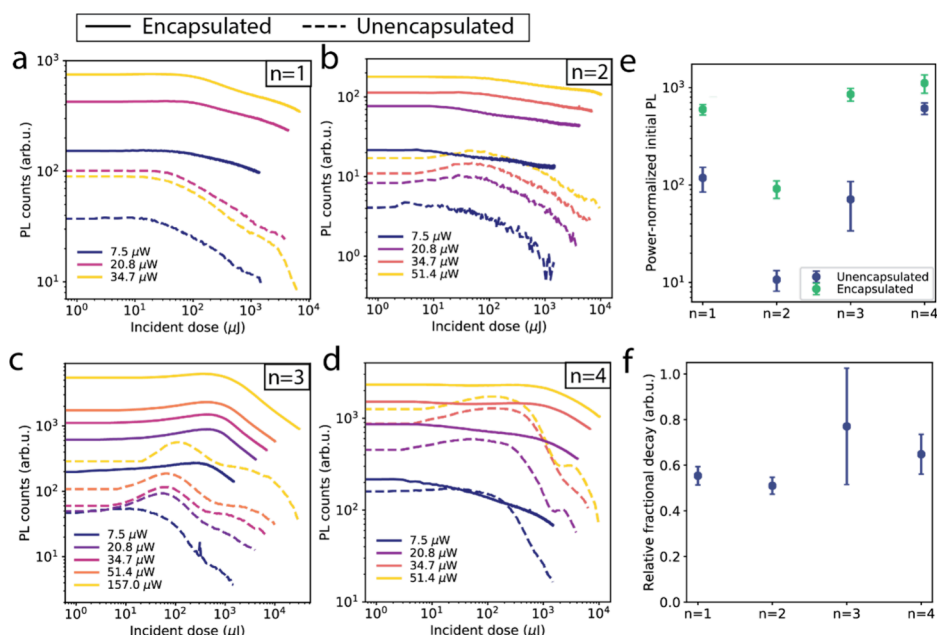
Figure 4. Impact of light-induced degradation on the PL of encapsulated and unencapsulated flakes. (a−d) PL intensity plotted as a function of the incident radiation dose (product of the laser power and the exposure time), for increasing laser power (darker to lighter) for encapsulated (continuous line) and unencapsulated samples (dashed line). (e) Intensity of the photoluminescence at the beginning of the exposure window, normalized by the laser power. Comparing values for the encapsulated and unencapsulated samples reveals an increased PL efficiency in the encapsulated samples. (f) Plot of the relative fractional decay, F_E/F_U, for the different n-values. The ratio remains below 1 for all n-values, indicating slower degradation dynamics in the encapsulated samples.
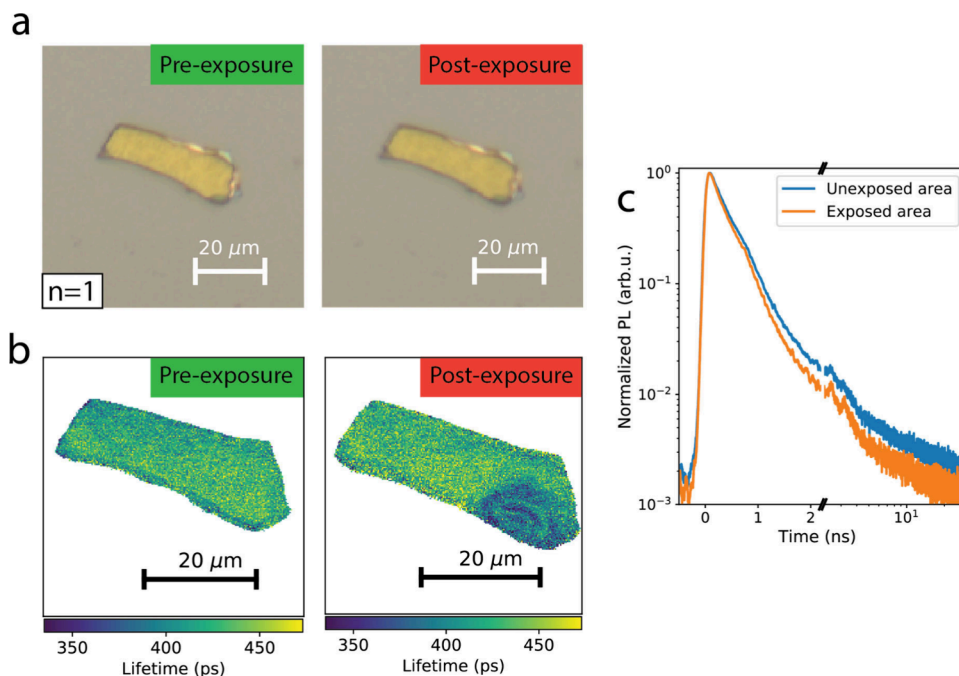

Figure 5. lifetime shortening in encapsulated flakes under illumination. (a) Optical images of an $n = 1$ 2D perovskite flake before and after local photoexcitation, showing no signs of morphology changes. (b) PL lifetime images before and after photoexcitation of the same flake shown in (a), showing the reduction of the lifetime in the photoexcited area. (c) Time-dependence of the PL signal in the exposed area and in a pristine area, showing a shortening of the lifetime in the exposed area.

exposure time multiplied by the incident power). The traces for the encapsulated samples (continuous lines) reveal that, for all n-values and all laser powers used, the PL signal decays as a function of the incident dose, indicating that the encapsulation does not fully prevent material degradation under illumination. We point out the presence of an initial PL increase at low

incident doses for the unencapsulated $n > 1$ flakes, likely associated with the passivating effect of oxygen molecules binding to iodide vacancies reported in 3D perovskites.[28,29]

Despite the presence of photodegradation in the encapsulated samples, a comparison with the unencapsulated samples (dashed lines) highlights the beneficial effect of encapsulation
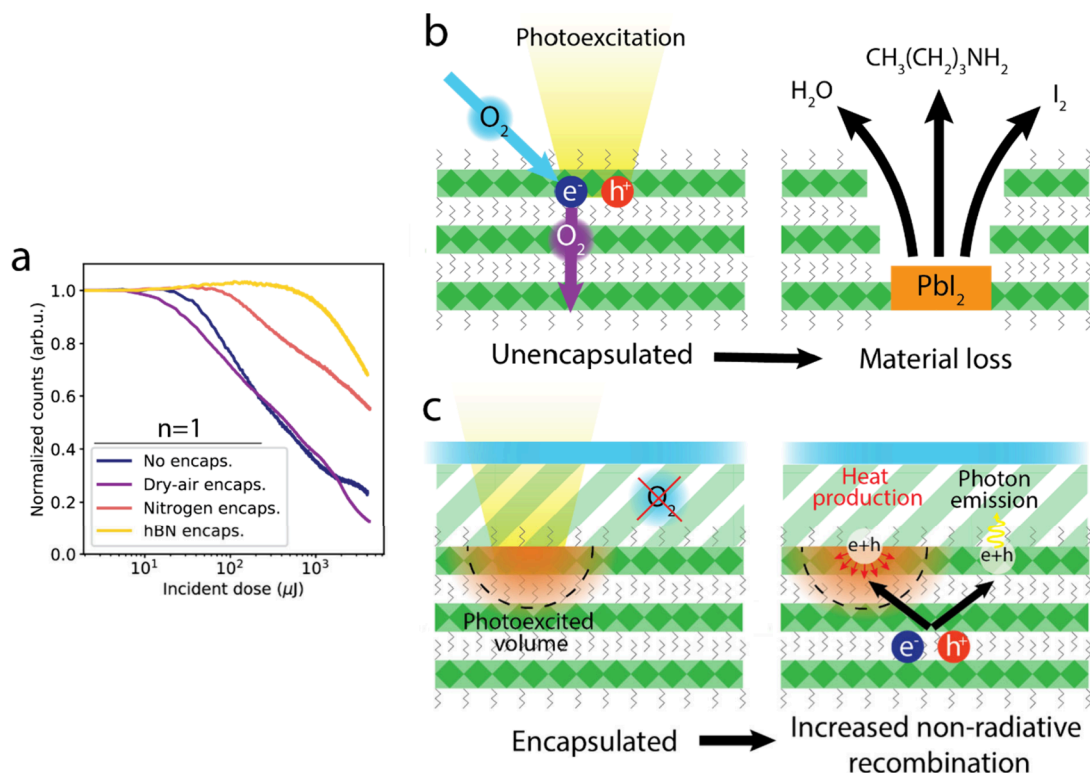
Figure 6. Passivation approaches and degradation mechanisms. (a) Comparison of PL decay traces obtained for $n = 1$ flakes in different environmental conditions, photoexcited with the same laser fluence. The comparison shows that stacking an hBN flake on top of the 2D perovskite flake and then encapsulating it in nitrogen leads to the highest photostability, while encapsulation in dry air (12.1% RH) does not improve the stability of the flakes. (b) Schematic representation of the proposed reaction mechanism in unencapsulated flakes, involving the formation of O_2^- species that react with the perovskite structure, inducing its decomposition. (c) Schematic representation of the photoinduced increase in nonradiative recombination proposed for the encapsulated flakes.

on the initial intensity of the PL signal. Figure 4e shows the initial PL intensity normalized by the laser power and averaged over the measurements with different power. The plot reveals that, regardless of the power used, encapsulation considerably improves the initial PL intensity, likely due to air-induced increase in nonradiative recombination occurring before the measurement.[22]

Furthermore, the encapsulation helps slow the rate of PL decay. To quantify this effect, we define the fractional PL decay as

$$F = \frac{PL_0 - PL_{final}}{PL_0} \tag{1}$$

where PL_0 indicates the initial PL intensity and PL_{final} is the PL intensity at the highest dose. This quantity represents the fractional loss of PL at the end of the exposure and can be used as an indicator of the severity of the degradation of PL intensity during the exposure time. We can then compare the degradation of encapsulated and unencapsulated samples by considering the ratio of the fractional decays F_E/F_U, where the E and U subscripts refer to the encapsulated and unencapsulated samples, respectively. Figure 4f shows F_E/F_U for the different n-values, with each data point averaged over measurements with different fluences (Figure S8). The ratio is below 1 for all n-values, indicating a decreased rate of degradation for the encapsulated flakes. Overall, the PL dynamics under illumination reveal that encapsulation, while slowing down the dynamics of PL losses, does not fully prevent
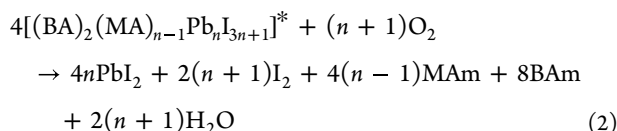
degradation of the electronic properties of the (quasi-) 2D perovskite flakes.

In the absence of a clear material loss mechanism, photoluminescence quenching is associated with increased nonradiative recombination. To investigate this effect locally, we measured time-resolved PL, monitoring for changes in the emission lifetime between exposed and pristine areas of the flakes (see Methods and Figure S9 in the Supporting Information for the description of the fit). Figure 5a,b shows optical and PL lifetime maps of the same $n = 1$ flake, both before (left) and after exposure (right). Even though the optical images do not show clear signs of morphological changes, the lifetime maps show the appearance of a region that exhibits a shorter lifetime after photoexcitation. A similar lifetime shortening is observed in Figure 5c, showing the time dependence of the PL integrated over the exposed spot and the pristine area. Fitting the data with a single exponential decay (Figure S10, Supporting Information) gives a lifetime of 431.0 ± 0.2 ps on the pristine area and 388.9 ± 0.2 ps in the exposed area. Since the PL decay is determined by the competition between radiative and nonradiative recombination, a shortening of the decay lifetime accompanied by a decrease in PL intensity indicates an increase in nonradiative recombination in the morphologically unaltered spots.

Having identified a clear difference between photodegradation processes affecting (quasi-) 2D perovskites in air and in nitrogen, we attempted to determine the relative contributions of oxygen and moisture to air-induced degradation. Figure 6a shows a comparison of the PL decay as a function of the incident dose for $n = 1$ flakes photoexcited with the same laser

power under different environmental conditions. While nitrogen encapsulation leads to a slower PL decay, repeating the same encapsulation procedure in dry air (12.1% relative humidity) did not show enhanced stability compared to that of the unencapsulated sample (photoexcited at 55% relative humidity). This observation suggests that oxygen plays a dominant role in triggering the rapid photodegradation of the material, although the role of water cannot be fully excluded. At the same time, the result indicates that the confinement of volatile degradation products in the encapsulation volume does not significantly affect the photostability of the flakes.

Analogous to the degradation pathways proposed for 3D perovskites,[30] we speculate that the photoinduced degradation of (quasi-) 2D perovskites follows the reaction

$$4[(BA)_2(MA)_{n-1}Pb_nI_{3n+1}]^* + (n + 1)O_2$$
$$\rightarrow 4nPbI_2 + 2(n + 1)I_2 + 4(n - 1)MAm + 8BAm$$
$$+ 2(n + 1)H_2O \tag{2}$$

with MAm and BAm indicating methylamine (CH_3NH_2) and butylamine ($CH_3(CH_2)_3NH_2$) species, MA and BA indicating methylammonium ($CH_3NH_3^+$) and butylammonium ($CH_3(CH_2)_3NH_3^+$) cations, and the asterisk indicating that the (quasi-) 2D perovskite material is in the photoexcited state. The reaction, schematically depicted in Figure 6b, involves the capture of a photoexcited electron by an oxygen molecule, leading to the formation of a reactive O_2^- species and its diffusion into the material. Upon exposure to O_2^-, the (quasi-) 2D perovskite decomposes, releasing volatile species (H_2O, I_2, MAm, and BAm) and leaving behind PbI_2.

In the absence of oxygen, the reaction described in eq 2 cannot happen. Consequently, photoexcitation under nitrogen leads mainly to an increase in nonradiative recombination channels, represented schematically in Figure 6c. Increased nonradiative recombination could be caused by carrier trapping at undercoordinated surface sites[31] or by the accumulation of mobile ions.[32,33] Despite the reduced severity of light-induced changes in the encapsulated flakes, further prevention of PL quenching might be the key to unlocking the full potential of these materials for spectroscopic investigations and device applications. To increase the photostability upon encapsulation, we stacked a flake of hexagonal boron nitride (hBN) on top of an $n = 1$ flake before encapsulating it in nitrogen (Figure S11), with the aim to simultaneously decrease the diffusion of residual oxygen into the flake and to passivate surface states.[22] The resulting PL decay upon photoexcitation (hBN passivation in Figure 6a) shows a remarkable stability increase, as the unencapsulated flake reaches the final PL intensity of the hBN-passivated flake after being exposed to a 30× lower incident dose. These results demonstrate the need for synergistic passivation strategies to prevent the degradation processes affecting these materials.

In conclusion, we have shown the presence of strong photodegradation processes affecting $n \leq 4$ (quasi-) 2D perovskites. Moreover, we have revealed the importance of oxygen for the degradation, proposing a reaction pathway and testing passivation strategies to suppress photodegradation. These results emphasize that the increased air-stability observed in 2D/3D solar cells should not be attributed to the intrinsic stability of quasi-2D perovskites and that a detailed understanding of the environment in which these

materials are placed is required to rationalize their evolution upon illumination.

ASSOCIATED CONTENT

Data Availability Statement

The data that support the findings of this study are available from the corresponding author upon reasonable request.

Ⓢ Supporting Information

The Supporting Information is available free of charge at https://pubs.acs.org/doi/10.1021/acsenergylett.4c02300.

Method section, additional figures, description of FTIR analysis, and description of photoluminescence lifetime fitting (PDF)

■ AUTHOR INFORMATION

Corresponding Author

Bruno Ehrler − Center for Nanophotonics, AMOLF, 1098 XG Amsterdam, The Netherlands; orcid.org/0000-0002-5307-3241; Email: ehrler@amolf.nl

Authors

Gianluca Grimaldi − Center for Nanophotonics, AMOLF, 1098 XG Amsterdam, The Netherlands; Optoelectronics Section, Cavendish Laboratory, University of Cambridge, Cambridge CB2 1TN, U.K.; orcid.org/0000-0002-2626-9118

Imme Schuringa − Center for Nanophotonics, AMOLF, 1098 XG Amsterdam, The Netherlands; orcid.org/0000-0002-8825-6937

Jaco J. Geuchies − Department of Molecular Spectroscopy, Max Planck Institute for Polymer Research, 55128 Mainz, Germany; orcid.org/0000-0002-0758-9140

Susan A. Rigter − Center for Nanophotonics, AMOLF, 1098 XG Amsterdam, The Netherlands; Van der Waals-Zeeman Institute, Institute of Physics, University of Amsterdam, Amsterdam 1098 XH, The Netherlands

Tom Hoekstra − Van der Waals-Zeeman Institute, Institute of Physics, University of Amsterdam, Amsterdam 1098 XH, The Netherlands

Jan Versluis − Center for Nanophotonics, AMOLF, 1098 XG Amsterdam, The Netherlands

Juanita Hidalgo − School of Materials Science and Engineering, Georgia Institute of Technology, Atlanta, Georgia 30332, United States; orcid.org/0000-0002-5832-3262

Juan-Pablo Correa-Baena − School of Materials Science and Engineering, Georgia Institute of Technology, Atlanta, Georgia 30332, United States; orcid.org/0000-0002-3860-1149

Jorik van de Groep − Van der Waals-Zeeman Institute, Institute of Physics, University of Amsterdam, Amsterdam 1098 XH, The Netherlands; orcid.org/0000-0003-3033-8005

Heejae Kim − Department of Molecular Spectroscopy, Max Planck Institute for Polymer Research, 55128 Mainz, Germany; Present Address: Pohang University of Science and Technology (POSTECH), 77 Cheongam-ro, Nam-gu, Pohang-si, Gyeongsangbuk-do, South Korea; orcid.org/0000-0002-9025-7322

Mischa Bonn − Department of Molecular Spectroscopy, Max Planck Institute for Polymer Research, 55128 Mainz, Germany; orcid.org/0000-0001-6851-8453

Complete contact information is available at:
https://pubs.acs.org/10.1021/acsenergylett.4c02300

■ **REFERENCES**

(1) Best Research-Cell Efficiency Chart. https://www.nrel.gov/pv/cell-efficiency.html (accessed 2024-07-08).

(2) Smith, I. C.; Hoke, E. T.; Solis-Ibarra, D.; McGehee, M. D.; Karunadasa, H. I. A Layered Hybrid Perovskite Solar-Cell Absorber with Enhanced Moisture Stability. *Angew. Chem., Int. Ed.* **2014**, *53* (42), 11232–11235.

(3) Grancini, G.; Roldán-Carmona, C.; Zimmermann, I.; Mosconi, E.; Lee, X.; Martineau, D.; Narbey, S.; Oswald, F.; De Angelis, F.; Graetzel, M.; Nazeeruddin, M. K. One-Year Stable Perovskite Solar Cells by 2D/3D Interface Engineering. *Nat. Commun.* **2017**, *8* (1), No. 15684.

(4) Ren, H.; Yu, S.; Chao, L.; Xia, Y.; Sun, Y.; Zuo, S.; Li, F.; Niu, T.; Yang, Y.; Ju, H.; Li, B.; Du, H.; Gao, X.; Zhang, J.; Wang, J.; Zhang, L.; Chen, Y.; Huang, W. Efficient and Stable Ruddlesden–Popper Perovskite Solar Cell with Tailored Interlayer Molecular Interaction. *Nat. Photonics* **2020**, *14* (3), 154–163.

(5) Shao, M.; Bie, T.; Yang, L.; Gao, Y.; Jin, X.; He, F.; Zheng, N.; Yu, Y.; Zhang, X. Over 21% Efficiency Stable 2D Perovskite Solar Cells. *Adv. Mater.* **2022**, *34* (1), No. 2107211.

(6) Chen, H.; Teale, S.; Chen, B.; Hou, Y.; Grater, L.; Zhu, T.; Bertens, K.; Park, S. M.; Atapattu, H. R.; Gao, Y.; Wei, M.; Johnston, A. K.; Zhou, Q.; Xu, K.; Yu, D.; Han, C.; Cui, T.; Jung, E. H.; Zhou, C.; Zhou, W.; Proppe, A. H.; Hoogland, S.; Laquai, F.; Filleter, T.; Graham, K. R.; Ning, Z.; Sargent, E. H. Quantum-Size-Tuned Heterostructures Enable Efficient and Stable Inverted Perovskite Solar Cells. *Nat. Photonics* **2022**, *16*, 352–358.

(7) Azmi, R.; Ugur, E.; Seitkhan, A.; Aljamaan, F.; Subbiah, A. S.; Liu, J.; Harrison, G. T.; Nugraha, M. I.; Eswaran, M. K.; Babics, M.; Chen, Y.; Xu, F.; Allen, T. G.; Rehman, A. ur; Wang, C.-L.; Anthopoulos, T. D.; Schwingenschlögl, U.; De Bastiani, M.; Aydin, E.; De Wolf, S. Damp Heat–Stable Perovskite Solar Cells with Tailored-Dimensionality 2D/3D Heterojunctions. *Science* **2022**, *376* (6588), 73–77.

(8) Zhao, X.; Liu, T.; Burlingame, Q. C.; Liu, T.; Holley, R.; Cheng, G.; Yao, N.; Gao, F.; Loo, Y.-L. Accelerated Aging of All-Inorganic, Interface-Stabilized Perovskite Solar Cells. *Science* **2022**, *377* (6603), 307–310.

(9) Mahmud, M. A.; Duong, T.; Peng, J.; Wu, Y.; Shen, H.; Walter, D.; Nguyen, H. T.; Mozaffari, N.; Tabi, G. D.; Catchpole, K. R.; Weber, K. J.; White, T. P. Origin of Efficiency and Stability Enhancement in High-Performing Mixed Dimensional 2D-3D Perovskite Solar Cells: A Review. *Adv. Funct. Mater.* **2022**, *32* (3), No. 2009164.

(10) Cao, D. H.; Stoumpos, C. C.; Farha, O. K.; Hupp, J. T.; Kanatzidis, M. G. 2D Homologous Perovskites as Light-Absorbing Materials for Solar Cell Applications. *J. Am. Chem. Soc.* **2015**, *137* (24), 7843–7850.

(11) Stoumpos, C. C.; Cao, D. H.; Clark, D. J.; Young, J.; Rondinelli, J. M.; Jang, J. I.; Hupp, J. T.; Kanatzidis, M. G. Ruddlesden−Popper Hybrid Lead Iodide Perovskite 2D Homologous Semiconductors. *Chem. Mater.* **2016**, *28* (8), 2852–2867.

(12) Wu, G.; Liang, R.; Ge, M.; Sun, G.; Zhang, Y.; Xing, G. Surface Passivation Using 2D Perovskites toward Efficient and Stable Perovskite Solar Cells. *Adv. Mater.* **2022**, *34* (8), No. 2105635.

(13) Tsai, H.; Nie, W.; Blancon, J.-C.; Stoumpos, C. C.; Asadpour, R.; Harutyunyan, B.; Neukirch, A. J.; Verduzco, R.; Crochet, J. J.; Tretiak, S.; Pedesseau, L.; Even, J.; Alam, M. A.; Gupta, G.; Lou, J.; Ajayan, P. M.; Bedzyk, M. J.; Kanatzidis, M. G.; Mohite, A. D. High-Efficiency Two-Dimensional Ruddlesden−Popper Perovskite Solar Cells. *Nature* **2016**, *536* (7616), 312–316.

(14) Cho, J.; DuBose, J. T.; Le, A. N. T.; Kamat, P. V. Suppressed Halide Ion Migration in 2D Lead Halide Perovskites. *ACS Materials Lett.* **2020**, *2* (6), 565–570.

(15) Akriti; Shi, E.; Shiring, S. B.; Yang, J.; Atencio-Martinez, C. L.; Yuan, B.; Hu, X.; Gao, Y.; Finkenauer, B. P.; Pistone, A. J.; Yu, Y.; Liao, P.; Savoie, B. M.; Dou, L. Layer-by-Layer Anionic Diffusion in Two-Dimensional Halide Perovskite Vertical Heterostructures. *Nat. Nanotechnol.* **2021**, *16*, 584–591.

(16) Chen, Z.; Xue, H.; Brocks, G.; Bobbert, P. A.; Tao, S. Thermodynamic Origin of the Photostability of the Two-Dimensional Perovskite PEA2Pb(I1−xBrx)4. *ACS Energy Lett.* **2023**, *8* (2), 943–949.

(17) Luo, Y.; Zhang, S.; Chen, J.-S.; Ma, X.; Ma, K.; Deng, J.; Jiang, Y.; Li, L.; Lai, B.; Chen, S.; Wieghold, S.; Dou, L. Photo-Induced Halide Redistribution in 2D Halide Perovskite Lateral Heterostructures. *Joule* **2023**, *7* (10), 2376–2385.

(18) Perini, C. A. R.; Rojas-Gatjens, E.; Ravello, M.; Mendez, A. F. C.; Hidalgo, J.; An, Y.; Kim, S.; Lai, B.; Li, R.; Acuña, C. S.; Correa-Baena, J.-P. Interface Reconstruction from Ruddlesden-Popper Structures Impacts Stability in Lead Halide Perovskite Solar Cells. *Adv. Mater.* **2022**, *34*, No. 2204726.

(19) Fang, H.-H.; Yang, J.; Tao, S.; Adjokatse, S.; Kamminga, M. E.; Ye, J.; Blake, G. R.; Even, J.; Loi, M. A. Unravelling Light-Induced Degradation of Layered Perovskite Crystals and Design of Efficient Encapsulation for Improved Photostability. *Adv. Funct. Mater.* **2018**, *28* (21), No. 1800305.

(20) Coriolano, A.; Polimeno, L.; De Giorgi, M.; Todisco, F.; Mastria, R.; Ardizzone, V.; Dominici, L.; Ballarini, D.; Rizzo, A.; Gigli, G.; Sanvitto, D.; De Marco, L. Improved Photostability in Fluorinated 2D Perovskite Single Crystals. *Nanomaterials* **2021**, *11* (2), 465.

(21) Hofstetter, Y. J.; García-Benito, I.; Paulus, F.; Orlandi, S.; Grancini, G.; Vaynzof, Y. Vacuum-Induced Degradation of 2D Perovskites. *Frontiers in Chemistry* **2020**, *8*, 1.

(22) Seitz, M.; Gant, P.; Castellanos-Gomez, A.; Prins, F. Long-Term Stabilization of Two-Dimensional Perovskites by Encapsulation with Hexagonal Boron Nitride. *Nanomaterials* **2019**, *9* (8), 1120.

(23) Myers, D. R.; Emery, K.; Gueymard, C. Revising and Validating Spectral Irradiance Reference Standards for Photovoltaic Performance Evaluation. *Journal of Solar Energy Engineering* **2004**, *126* (1), 567–574.

(24) Aristidou, N.; Sanchez-Molina, I.; Chotchuangchutchaval, T.; Brown, M.; Martinez, L.; Rath, T.; Haque, S. A. The Role of Oxygen in the Degradation of Methylammonium Lead Trihalide Perovskite Photoactive Layers. *Angew. Chem.* **2015**, *127* (28), 8326–8330.

(25) Manser, J. S.; Saidaminov, M. I.; Christians, J. A.; Bakr, O. M.; Kamat, P. V. Making and Breaking of Lead Halide Perovskites. *Acc. Chem. Res.* **2016**, *49* (2), 330–338.

(26) Huang, J.; Tan, S.; Lund, P. D.; Zhou, H. Impact of H2O on Organic−Inorganic Hybrid Perovskite Solar Cells. *Energy Environ. Sci.* **2017**, *10* (11), 2284–2311.

(27) Brenes, R.; Eames, C.; Bulović, V.; Islam, M. S.; Stranks, S. D. The Impact of Atmosphere on the Local Luminescence Properties of Metal Halide Perovskite Grains. *Adv. Mater.* **2018**, *30* (15), No. 1706208.

(28) Andaji-Garmaroudi, Z.; Anaya, M.; Pearson, A. J.; Stranks, S. D. Photobrightening in Lead Halide Perovskites: Observations, Mechanisms, and Future Potential. *Adv. Energy Mater.* **2020**, *10* (13), No. 1903109.

(29) Huang, L.; Ge, Z.; Zhang, X.; Zhu, Y. Oxygen-Induced Defect-Healing and Photo-Brightening of Halide Perovskite Semiconductors: Science and Application. *Journal of Materials Chemistry A* **2021**, *9* (8), 4379−4414.

(30) Aristidou, N.; Eames, C.; Sanchez-Molina, I.; Bu, X.; Kosco, J.; Islam, M. S.; Haque, S. A. Fast Oxygen Diffusion and Iodide Defects Mediate Oxygen-Induced Degradation of Perovskite Solar Cells. *Nat. Commun.* **2017**, *8* (1), No. 15218.

(31) Liu, L.; Deng, L.; Huang, S.; Zhang, P.; Linnros, J.; Zhong, H.; Sychugov, I. Photodegradation of Organometal Hybrid Perovskite Nanocrystals: Clarifying the Role of Oxygen by Single-Dot Photoluminescence. *J. Phys. Chem. Lett.* **2019**, *10* (4), 864−869.

(32) Chen, S.; Wen, X.; Huang, S.; Huang, F.; Cheng, Y.-B.; Green, M.; Ho-Baillie, A. Light Illumination Induced Photoluminescence Enhancement and Quenching in Lead Halide Perovskite. *Solar RRL* **2017**, *1* (1), No. 1600001.

(33) Chen, S.; Wen, X.; Sheng, R.; Huang, S.; Deng, X.; Green, M. A.; Ho-Baillie, A. Mobile Ion Induced Slow Carrier Dynamics in Organic−Inorganic Perovskite CH3NH3PbBr3. *ACS Appl. Mater. Interfaces* **2016**, *8* (8), 5351−5357.